Journal of Medicinal Chemistry Article

J. Med. Chem. **2010,** *53,* 1673–1685 **1673**
DOI: 10.1021/jm901450d

5-OMe-UDP is a Potent and Selective $P2Y_6$-Receptor Agonist

Tamar Ginsburg-Shmuel,[†] Michael Haas,[‡] Marlen Schumann,[‡] Georg Reiser,[‡] Ori Kalid,[†] Noa Stern,[†] and Bilha Fischer*[,†]

[†]*Department of Chemistry, Gonda-Goldschmied Medical Research Center, Bar-Ilan University, Ramat-Gan 52900, Israel and*
[‡]*Institute for Neurobiochemistry, Faculty of Medicine, Otto von Guericke University, Leipziger Str. 44 D-39120 Magdeburg, Germany*

Received September 30, 2009

P2Y nucleotide receptors (P2Y-Rs) play important physiological roles. However, most of the P2Y-R subtypes are still lacking potent and selective agonists and antagonists. Based on data mining analysis of binding interactions in 44 protein−uridine nucleos(t)ides complexes, we designed uracil nucleotides, substituted at the C5/C6 position. All C6-substituted derivatives were inactive at the $P2Y_{2,4,6}$-Rs, while out of the C5-substituted analogues, only 5-OMe-UD(T)P showed activity. To rationalize the data, the ionization and conformation of these analogues were evaluated. The pK_a values of most analogues substituted at the C5/C6 positions were unaltered compared to UTP (pK_a 9.42), except for 5-F-UTP nucleotide (pK_a 7.85). C6-substituted analogues adopt the *syn* or *high-syn* conformations, which are disfavored by the receptors, while 5-OMe-UD(T)P adopt the favored *anti* conformation. Furthermore, 5-OMe-UDP adopts the *S* sugar puckering, which is the conformation preferred by the $P2Y_6$-R, but not the $P2Y_2$- or $P2Y_4$-Rs. 5-OMe-UDP fulfills the conformational and H-bonding requirements of $P2Y_6$-R, thus, making a potent $P2Y_6$-R agonist (EC_{50} 0.08 μM), more than UDP (EC_{50} 0.14 μM).

Introduction

The members of the P2 receptor (P2R[a]) superfamily, consisting of ligand-gated ion channels (P2X-Rs) and G protein-coupled receptors (P2Y-Rs), are activated by endogenous extracellular nucleotides.[1] Eight human P2Y-Rs subtypes are known so far ($P2Y_1$, $P2Y_2$, $P2Y_4$, $P2Y_6$, $P2Y_{11}$−$P2Y_{14}$). The $P2Y_{2,4,6}$-Rs are the only P2Y-R subtypes activated by uracil nucleotides, while the $P2Y_{1,2,11}$ receptors are activated by adenine nucleotides (ATP, **1**, or ADP, **2**). $P2Y_2$-R is activated by **1** as well as UTP, **3**, with similar potency, $P2Y_4$-R is activated only by **3** and $P2Y_6$-R is a UDP, **4**, receptor (Figure 1).

$P2Y_{2,4,6}$-Rs play important physiological roles.[1] For example, activation of the $P2Y_2$-R induces mucous clearance in lungs (having potential relevance for the treatment of cystic fibrosis),[2] ocular surface hydration,[3] inflammation induction and immunomodulation,[4] as well as proliferation of tumor cells.[5] Similarly to the $P2Y_2$-R, the $P2Y_4$-R has a role in vasodilatation, and regulation of epithelial chloride transport and might be considered as a target in the treatment of cystic fibrosis.[6] The $P2Y_6$-R is involved in several functions in the immune system[7] and has been shown to be expressed in inflammatory bowel disease infected cells.[8]

Most of the P2Y-R subtypes are still lacking potent and selective synthetic agonists and antagonists. To date the development of agonists for the $P2Y_{2/4/6}$-Rs has mainly included modification of the different moieties of **1**, **3**, and **4**: the phosphate ring, ribose, and base.[9] Lately, the structure−activity relationship, molecular modeling, and mutagenesis studies for agonists and antagonists at the $P2Y_{2/4/6}$-Rs have been extensively investigated.[10−12] Different uracil modifications have been performed over the past few years in an attempt to identify agonists that will prove to be more potent than the endogenous ligands **1**, **3**, and **4**.

Some promising synthetic agonists for each of the uridine nucleotide receptors have been recently identified. Examples of such compounds, active at the $P2Y_2$-R, include Up_4U (INS365, Diquafosol), **5**, and Up_4dC (INS37217, Denufosol), **6** (Figure 2). Both dinucleotides **5** and **6** are at phase 3 clinical trials for the treatment of dry eye disease and cystic fibrosis, respectively.[13] 2′-Amino-2-thio-UTP, **7**, combines two modifications which enhance both potency and selectivity at the $P2Y_2$-R, probably due to additional interactions of the 2′-amino group with F6.51 and Y3.33, as well as interactions of the sulfur atom at position 2 with Y1.39.[14] 5-Alkyl-substituted UTP derivatives, for example, 5-ethyl UTP, **8**, were full agonists at the $P2Y_2$-R, but were all less potent than **3**.[15] Introduction of a bromine atom at the 5-position of UTP, **9**, led to a 15-fold decrease in activity at the $P2Y_2$-R.[15]

At the $P2Y_4$-R, the 5-bromo substitution greatly reduced activity.[10] However, at the $P2Y_6$-R, both 5-Br-UTP, **9**,[16] and 5-Br-UDP, **10**,[17] were potent agonists, because the $P2Y_6$-R is more tolerant to substituents at position 5.

UDP-β-S, **11**, was found to be more potent than **4** in activation of the $P2Y_6$-R.[12] At the $P2Y_6$-R, 5-iodo-UDP (MRS2693), **12**,[7] was equipotent to **4** and the dinucleoside triphosphate INS48823, **13**, was a potent and stable agonist.[18]

Assessment of the pharmacological activity of methano-carba-UTP and UDP analogues, **14** and **15**, respectively, together with molecular modeling studies, have shown that

*Corresponding author. Fax: 972-3-6354907. Tel.: 972-3-5318303. E-mail: bfischer@mail.biu.ac.il.

[a]Abbreviations: P2R, P2 receptor; ATP, adenosine triphosphate; ADP, adenosine diphosphate; UTP, uridine triphosphate; UDP, uridine diphosphate; P2Y-R, P2Y-receptor; PDB, protein data bank; EDG, electron donating group; EWG, electron withdrawing group; SAR, structure−activity relationship; TEAB, triethylammonium bicarbonate; HPFC, high-performance FLASH chromatography; TEAA, triethylammonium acetate; MALDI, matrix-assisted laser desorption/ionization; PSI-BLAST, position specific iterative BLAST; GFP, green fluorescent protein; cDNA; complementary DNA.

Published on Web 01/22/2010

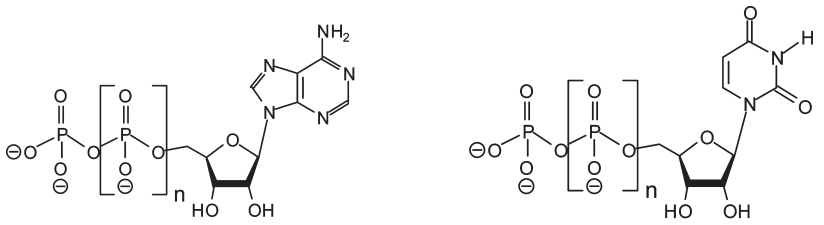

1 n = 2
2 n = 1

3 n = 2
4 n = 1

Figure 1. Endogenous agonists of P2Y-Rs.

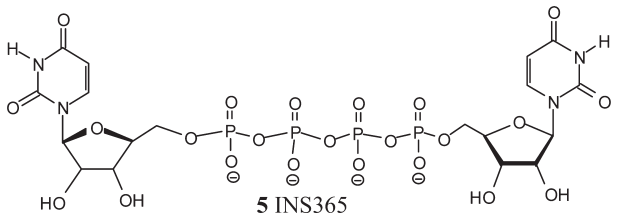

5 INS365
EC_{50} ($P2Y_2$-R) = 0.10
(UTP = 0.03)

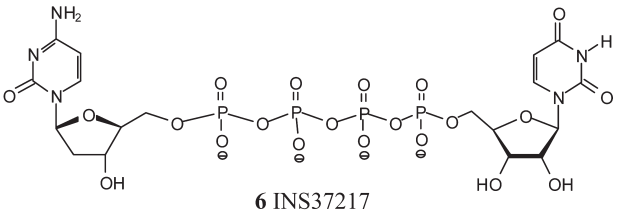

6 INS37217
EC_{50} ($P2Y_2$-R) = 0.22
(UTP = 0.03)

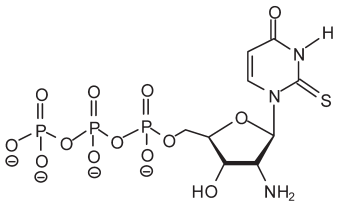

7 2'-amino-2-thio-UTP
EC_{50} ($P2Y_2$-R) = 0.008
(UTP = 0.049)

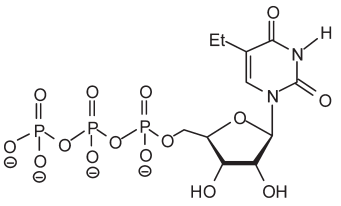

8 5-Et-UTP
EC_{50} ($mP2Y_2$-R) = 99[c]
(UTP = 1.25)

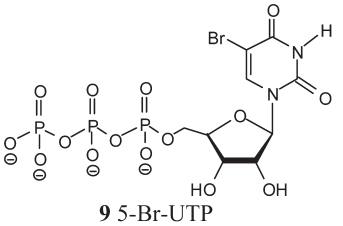

9 5-Br-UTP
EC_{50} ($P2Y_2$-R) = 2.06 (UTP = 0.14)
EC_{50} ($P2Y_4$-R) = 10 (UTP = 0.35)
EC_{50} ($P2Y_6$-R) = 0.8 (UDP = 0.3)

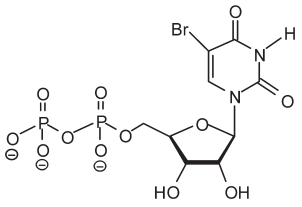

10 5-Br-UDP
EC_{50} ($rP2Y_6$-R) = 0.13[d]
(UDP = 0.19)

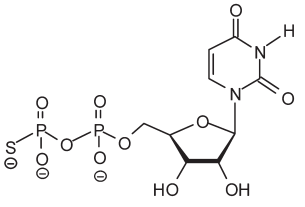

11 UDP-β-S
EC_{50} ($P2Y_6$-R) = 0.047
(UDP = 0.3)

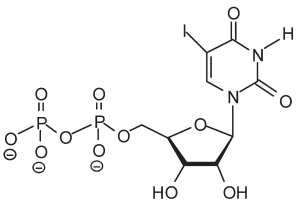

12 5-I-UDP
EC_{50} ($P2Y_6$-R) = 0.013
(UDP = 0.015)

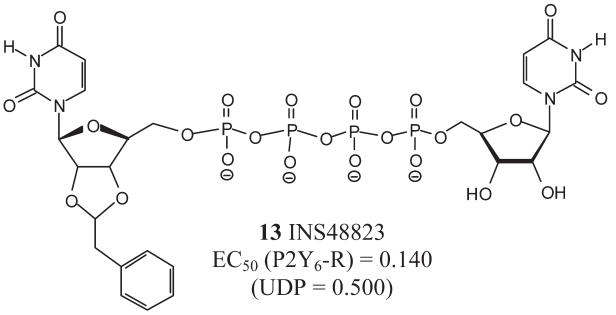

13 INS48823
EC_{50} ($P2Y_6$-R) = 0.140
(UDP = 0.500)

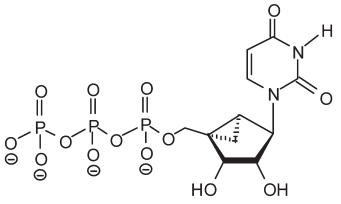

14 (*N*)-Methanocarba-UTP
EC_{50} ($P2Y_2$-R) = 0.0159
(UDP = 0.008)

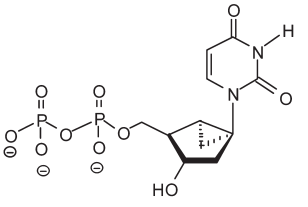

15 (*S*)-Methanocarba-2'-deoxy-UDP
EC_{50} ($P2Y_6$-R) = 0.23
(UDP = 0.013)

Figure 2. Known $P2Y_{2/4/6}$-Rs agonists and their EC_{50} values (in μM), compared to those of **3** or **4**. [a]EC_{50} values are for human P2Y-Rs unless otherwise noted. [b]For references for EC_{50} values see Introduction. [c]m = mouse P2Y-R. [d]r = rat P2Y-R.

while the $P2Y_2$-R and $P2Y_4$-R prefer the *N* (northern) conformation of the ribose ring, the *S* (southern) conformation is the one preferred by the $P2Y_6$-R.[7,19,20]

To date, hardly any of the synthesized nucleotides were more potent than the endogenous uracil nucleotides at the $P2Y_{2,4,6}$ receptors. The challenge of discovering new highly

potent and selective agonists remains unmet, especially for the $P2Y_{4/6}$-Rs. In addition, there is a need for partial agonists, since they can be used for the development of antagonists, which are currently almost lacking.

In this study, we attempted to design potent uridine nucleotide receptor agonists, by utilizing a data-mining approach. Specifically, we studied complexes of uracil-nucleos(t)ide -binding-proteins available in the PDB and identified the nucleos(t)ide recognition pattern. The data-mining results enabled us to design several UT(D)P analogues, where the nature/position of the uracil substituents was expected to enhance binding interactions with $P2Y_{2/4/6}$-Rs.

In this report, we describe the design and synthesis of analogues **16**−**22** and their activity at the $P2Y_{2,4,6}$ receptors. In addition, the biochemical activity of the analogues was correlated with parameters such as pK_a values and nucleotide conformation. Finally, we report the identification of 5-OMe-UDP, **21**, as a potent and selective $P2Y_6$-R agonist.

Results

Design of Uracil Nucleotides as Potential $P2Y_{2/4/6}$-Rs Agonists. Our approach of rational design of $P2Y_{2/4/6}$-Rs agonists involved data-mining analysis of 44 complexes of uracil-nucleoside/nucleotide-binding-proteins available in the PDB. The study of these complexes provided insights regarding recognition patterns in uracil-nucleos(t)ide binding proteins (Table 1, Supporting Information).

In the great majority of structures (79%), both ribose hydroxyls were engaged in hydrogen bonding. A small fraction of these interactions were water-mediated. A total of 92% of all ribose O2′ atoms were involved in H-bonds, of which a mere 7% were water mediated. A total of 82% of all ribose O3′ atoms were involved in H-bonds, of which a mere 9% were water-mediated. All except two ribose conformations were within the *N* and *S* domains, with the *S* domain considerably more abundant (29 *S* conformations, compared to 8 *N* conformations). In all but one of the structures, the base was in the *anti* conformation with respect to the ribose ring.

Regarding the uracil base, the results showed that molecular recognition of the uracil moiety in uracil-nucleos(t)ide involves the following interactions: (1) Hydrogen bonds, which are the most dominant interaction between the uracil base and its binding proteins. The most abundant hydrogen bond interaction, present in 98% of the structures, was between the uracil N3−H and a protein H-bond acceptor. The uracil O2 and O4 act as H-bond acceptors in 80 and 93% of the cases, respectively. (2) Interactions ($\pi-\pi$) between the uracil base and aromatic residues in the proteins, such as Phe, Trp, and Tyr, were found in 59% of the inspected structures; (3) π-Cation interactions between the uracil base and positively charged residues in the proteins, such as Lys and Arg, were detected in 25% of the complexes (Figure 3).

Based on the above findings, we hypothesized that electron donating groups (EDGs) at the uracil C5 and C6 positions would enhance the ligand−receptor interactions, possibly forming tight-binding agonists for P2Y uridine−nucleotide binding receptors.

Specifically, an electron donating group at the uracil C5 and/or C6 position was expected to increase the electron density in the ring, thus enhancing $\pi-\pi$ and π-cation interactions. In addition, hydrogen bonds were expected to be enhanced by substituting the C6 position in the uracil ring

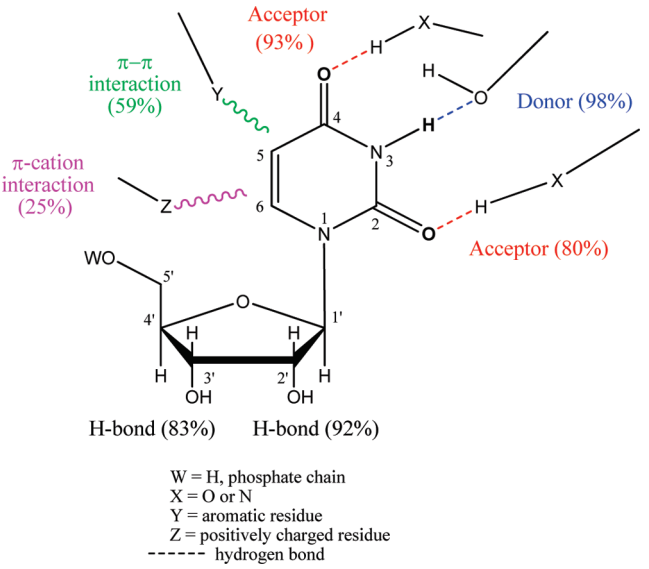

Figure 3. Recognition patterns in uracil−nucleos(t)ide binding proteins derived from data mining analysis of 44 complexes of uridine nucleos(t)tides and proteins using PDB files. Numerical values in brackets represent percentages of occurrences of H-bonding/$\pi-\pi$ interactions/π-cation interactions in the set of complexes studied.

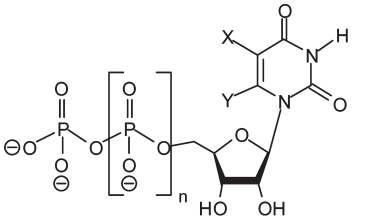

16	X = H	Y = SPh	n = 2
17	X = H	Y = SMe	n = 2
18	X = H	Y = OMe	n = 2
19	X = OMe	Y = H	n = 2
20	X = F	Y = H	n = 2
21	X = OMe	Y = H	n = 1
22	X = F	Y = H	n = 1

Figure 4. UDP and UTP analogues studied here.

with an electron donating group, which increases the electron density around the hydrogen bond acceptor O4. Enhanced H-bonding could also be expected upon substitution of electronegative atoms at C5, which would inductively increase the $\delta+$ character of N3−H, thus, making it a better H-bond donor.

Therefore, based on the above considerations, we designed a series of UTP and UDP analogues, where the C5 or C6 positions were substituted with ethers, thioethers, or F groups (**16**−**22**; Figure 4).

Synthesis of Potential $P2Y_{2/4/6}$-Rs Ligands. Synthesis of 6-Substituted Uridine Derivatives. 6-SPh-uridine, **23**, 6-SMe-uridine, **24**, were synthesized according to literature.[21−26] 6-OMe-uridine, **25**, was obtained in 43% yield from **23** by the addition of sodium methoxide in dry MeOH at RT for 2.5 days.

5′-Triphosphorylation of Nucleosides 23−**27.** The unprotected uridine derivatives were used for the preparation of the corresponding nucleotides by a one-pot 5′-triphosphorylation reaction (Scheme 1).[27]

First, $POCl_3$ was added at −15 °C to nucleosides **23**−**27** in trimethylphosphate to generate intermediate **28**.

Scheme 1. 5′-Triphosphorylation of Uridine Nucleosides **23**−**27**[a]

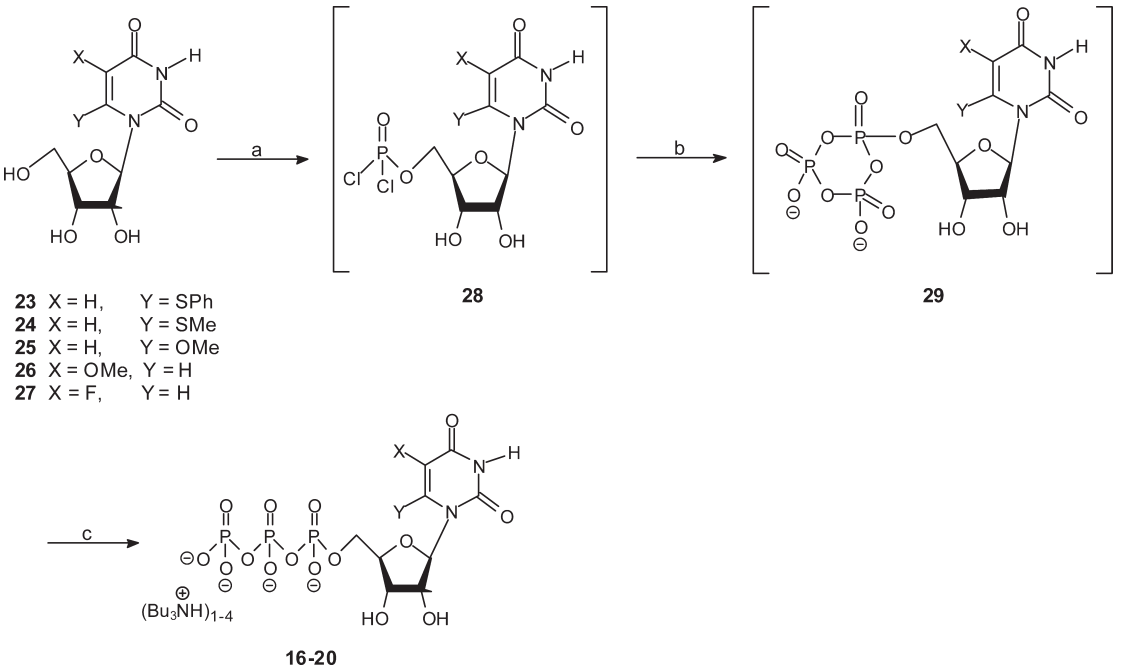

[a] Reagents and conditions: (a) (1) proton sponge, trimethylphosphate, −15 °C, 20 min; and (2) $POCl_3$, −15 °C, 2 h; (b) 1 M $P_2O_7H_2^{2-}(Bu_3N^+H)_2$ in dry DMF, Bu_3N, RT, −15 °C, 6 min; (c) 1 M TEAB, pH 7, RT, 45 min.

Scheme 2. 5′-Di-phosphorylation of Uridine Nucleosides **26** and **27**[a]

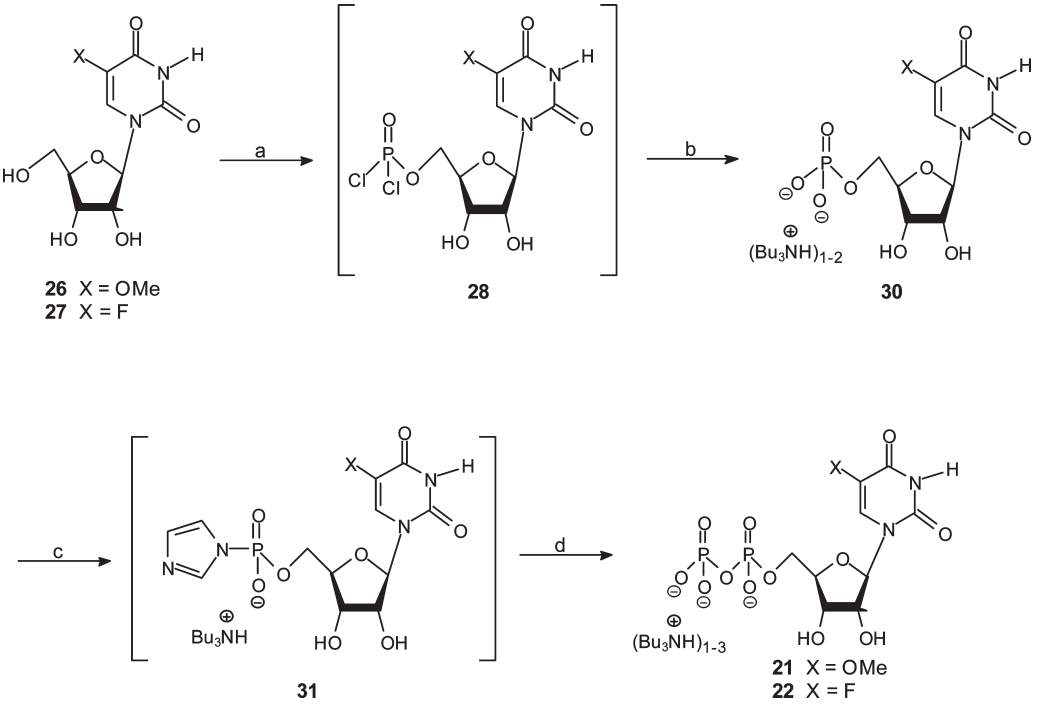

[a] Reagents and conditions: (a) (1) proton sponge, trimethylphosphate, −15 °C, 20 min; and (2) $POCl_3$, −15 °C, 2 h; (b) TEAB 1 M, pH 7, RT, 45 min, Bu_3N, RT, −15 °C, 6 min; (c) carbodiimidazole, dry DMF, RT, 3 h; (d) (1) dry MeOH, RT, 5 min; and (2) 1 M $PO_4H^-(Bu_3N^+H)_2$ in dry DMF, RT, 1 day.

Subsequently, the pyrophosphate tributyl ammonium salt in dry DMF was added at −15 °C and the reaction mixture was stirred for 6 min to form intermediate **29**. Finally, intermediate **29** was hydrolyzed in a TEAB buffer to yield nucleotides **16**−**20**. Purification of the nucleotides included ion-exchange LC followed by final purification by HPLC.

5′-Diphosphorylation of Nucleosides. 5-Substituted uridine analogues **26** and **27** were used for the preparation of their diphosphate analogues (Scheme 2). First, the nucleosides were reacted with $POCl_3$ to form intermediate **28**, which upon hydrolysis provided the monophosphate derivative **30**. Following LC purification, both NH_4^+ counterions of compound **30** were replaced by one Bu_3NH^+ ion and one Oct_3NH^+ ion. Subsequently, analogue **30** was treated with CDI to generate intermediate **31**. Finally, the phosphate bis(tributyl ammonium) salt in dry

DMF was added to produce the diphosphate products **21** and **22**.

Evaluation of Uridine Nucleotide Analogues 16−22 as $P2Y_{2/4/6}$-Rs Ligands. To study the activity of nucleotides **16−22** at the $P2Y_{2/4/6}$-Rs, we evaluated $[Ca^{2+}]_i$ mobilization induced by these analogues and compared it to that of **3** and **4**. These studies were performed in 1321N1 astrocytoma cells that were stably transfected with $P2Y_{2/4/6}$ receptors. Concentration−response curves were derived for a range of nucleotide concentrations, usually from 10^{-8} M to at least 10^{-5} M and, in some cases, up to 10^{-4} M when possible. The results are shown in Figure 5 and summarized in Table 1. In control measurements we found that untransfected 1321N1 astrocytoma cells did not show a response to any of the tested nucleotides (data not shown).

Neither 6-SPh-UTP, **16**, nor 6-SMe-UTP, **17**, exhibited any activity at any of the tested receptor subtypes. Yet, 6-OMe-UTP, **18**, showed some activity at the $P2Y_2$-R. Since no plateau was reached, the EC_{50} value was estimated to be approximately 3 μM. 5-OMe-UTP, **19**, exhibited a clear preference for the $P2Y_6$-R, with an EC_{50} value of 0.9 μM, which is about 6-fold higher than the EC_{50} value of the standard agonist **4**. 5-OMe-UTP, **19**, showed activity at the $P2Y_2$-R as well. Because no plateau was reached, the EC_{50} value was estimated to be around 2 μM. 5-OMe-UTP, **19**, was found to be not active at the $P2Y_4$-R. 5-F-UTP, **20**, acted as a potent agonist on two tested receptor subtypes, revealing its highest activity at the $P2Y_4$-R (EC_{50} 0.6 μM). The EC_{50} value for the $P2Y_2$-R is 10-fold higher. At the $P2Y_4$-R, 5-F-UTP, **20**, acted as a partial agonist. At the $P2Y_6$-R, 5-F-UTP, **20**, was found to be not active, at concentrations up to 100 μM. 5-OMe-UDP, **21**, exhibited a clear preference for the $P2Y_6$-R (EC_{50} 0.08 μM), and its potency was almost 2-fold higher than that of the endogenous $P2Y_6$-R agonist, UDP (EC_{50} 0.14 μM). The activity of the nucleotide reaches a first plateau at nucleotide concentrations ranging from 1 to 10 μM (Figure 5C, black circles), followed by a second phase of increased activity, at increasing nucleotide concentrations (Figure 5C, black circles: A concentration−response curve was calculated only for the first phase of increase; The number of data points was too low to calculate a concentration−response curve of the second phase). Therefore, a biphasic response pattern was deduced. 5-OMe-UDP, **21**, was completely inactive at the $P2Y_2$-R at concentrations up to 100 μM. 5-F-UDP, **22**, acted as an agonist on all three tested receptor subtypes. It is a partial agonist at the $P2Y_2$-R, $P2Y_4$-R, and $P2Y_6$-R, with EC_{50} values of 2, 3.5, and 10 μM, respectively. The maximal response at these receptor subtypes is about 50% of the maximal response achieved by the standard agonists.

At the $P2Y_2$-R, the most potent of the tested nucleotides is the standard agonist **3**. 5-F-UDP, **22**, acted as a partial agonist, with an EC_{50} value 20-fold higher than for UTP. 5-F-UTP, **20**, exhibited a 60-fold lower potency than **3**. A plateau was not reached for 5-OMe-UTP, **19**, and 6-OMe-UTP, **18**, within the range of nucleotide concentrations tested. 6-SPh-UTP, **16**, 6-SMe-UTP, **17**, and 5-OMe-UDP, **21**, evoked no response at all.

At the $P2Y_4$-R, 5-F-UTP, **20**, and the standard agonist **3** exhibit equal potency. This is followed by 5-F-UDP, **22**, with an EC_{50} value 7-fold higher than for **3**. For 5-OMe-UDP, **21**, no plateau was reached within the range of nucleotide concentrations tested, but the EC_{50} value is at least 40-fold higher than for UTP. 5-F-UTP, **20**, and 5-F-UDP, **22**, both act as partial agonists, evoking about 50% of the maximal UTP response. 6-SPh-UTP, **16**, 6-SMe-UTP, **17**, 6-OMe-UTP, **18**, 5-OMe-UTP, **19**, and 5-OMe-UDP, **21**, were not active.

At the $P2Y_6$-R, 5-OMe-UDP, **21**, is the most potent nucleotide, with a biphasic response. The plateau of the

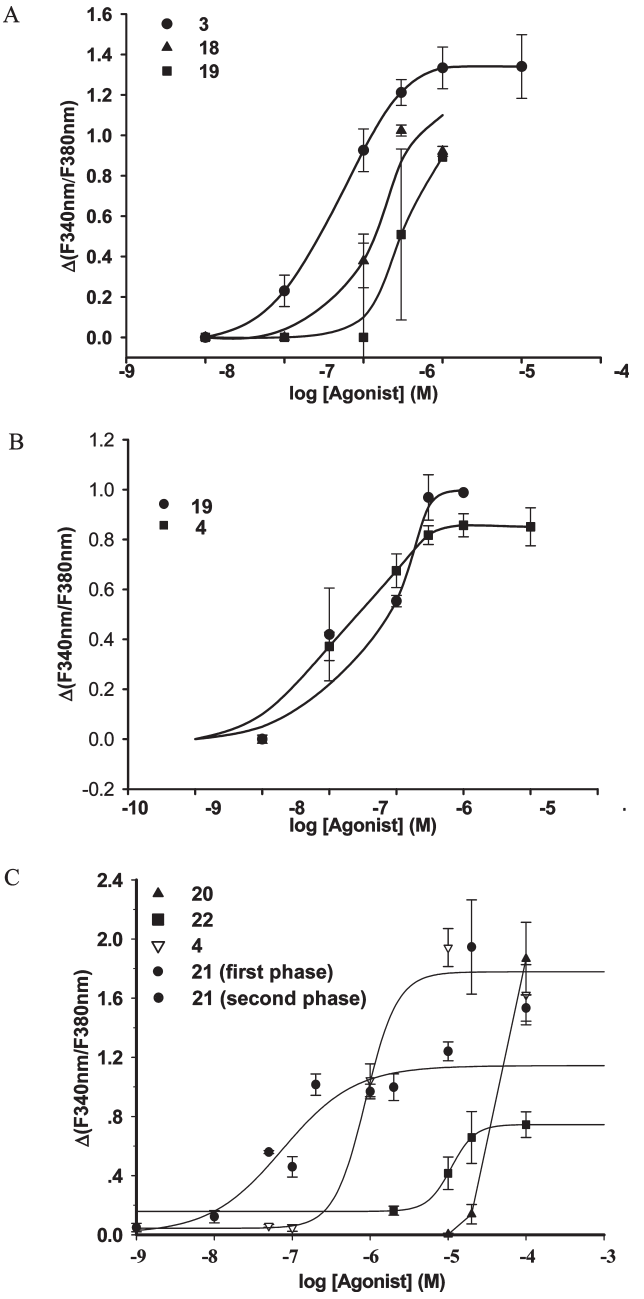

Figure 5. Activity of analogues **18−22** at the $P2Y_{2/6}$-receptors. 1321N1 cells stably expressing the $P2Y_{2/6}$ receptor GFP fusion protein, preincubated with 2 μM fura-2-AM, were stimulated with varying concentrations of agonists and the change in fluorescence (ΔF340 nm/F380 nm) was detected. Data represent the mean values and standard error from 20 to 60 cells. Data were obtained from at least three experiments. (A) Concentration−response curves for **3**, 6-OMe-UTP, **18**, and 5-OMe-UTP, **19**, at the human $P2Y_2$ receptor. (B) Concentration−response curves for **4** and 5-OMe-UTP, **19**, at the human $P2Y_6$ receptor. (C) Concentration−response curves for **4**, 5-F-UTP, **20**, 5-OMe-UDP, **21**, and 5-F-UDP, **22**, at the human $P2Y_6$ receptor. For **21**, concentrations higher than 10 μM values given by gray circles indicate a putative second phase of increase of $[Ca^{2+}]_i$. A concentration−response curve was calculated only for the first phase of increase.

Table 1. Potencies of Nucleotides **16**−**22** at $P2Y_{2/4/6}$-R, **3** at $P2Y_2$-R and $P2Y_4$-R, and **4** at $P2Y_6$-R[a]

agonist	EC_{50} values (μM)		
	$P2Y_2$-R	$P2Y_4$-R	$P2Y_6$-R
UTP (**3**)	0.1	0.5	n.m.[b]
UDP (**4**)	n.m.[b]	n.m.	0.14
6-SPh-UTP (**16**)	n.d.r.[c]	n.d.r.	n.d.r.
6-SMe-UTP (**17**)	response only at 10 μM[d]	n.d.r.	n.d.r.
6-OMe-UTP (**18**)	3[e]	n.d.r.	n.d.r.
5-OMe-UTP (**19**)	2[e]	response only at 10 μM[d]	0.9
5-F-UTP (**20**)	6	0.6[f]	response only at 100 μM[g]
5-OMe-UDP (**21**)	n.d.r.	≥20[h]	0.08[i]
5-F-UDP (**22**)	2[f]	3.5[f]	10[f]

[a] The EC_{50} values for $[Ca^{2+}]_i$ elevation were obtained from concentration−response curves based on fura-2/AM F340 nm/F380 nm ratio measurements.[46] [b] n.m. = not measured. [c] n.d.r. = no detectable response. [d] Only at 10 μM was a sporadic response detected in a minor group of cells tested. This may be due to some heterogeneity of the cells. [e] Measurements were conducted up to 10 μM of nucleotide concentration, where still no plateau was reached. For technical reasons no further measurements were possible. The EC_{50} values were estimated from these data. [f] The maximal response, a plateau in the concentration−response curve, reaches about 50% of the maximal receptor response obtained with the standard agonist **3** for $P2Y_2$-R and $P2Y_4$-R and **4** for $P2Y_6$-R. The EC_{50} value is derived from this concentration−response curve. Partial agonist activity is suggested. [g] Only at 100 μM was a sporadic response detected in a minor group of cells tested. This may be due to some heterogeneity of the cells. [h] Measurements were conducted up to 50 μM of nucleotide concentration, where still no plateau was reached. For technical reasons, no further measurements were possible. The EC_{50} values were estimated from these data. [i] The concentration−response curve reaches a first plateau at nucleotide concentrations from 1 to 10 μM (Figure 5C, black circles). This plateau level was at about 60% of the maximal receptor response obtained with the standard agonist. This is followed by a second phase of increases at increasing nucleotide concentrations (Figure 5C, black circles). Therefore, a biphasic response pattern is deduced. The EC_{50} value given is derived for the high affinity component of the biphasic response.

higher affinity component of the biphasic concentration−response curve is at about 60% of the maximal response of the standard agonist **4**. 5-OMe-UDP, **21**, therefore acts as an agonist at these concentrations. The potency of the standard agonist UDP is lower and 5-OMe-UTP, **19**, is about 6 times less potent than **4**. The potency of 5-F-UDP, **22**, is about 70-fold lower than for **4** and it acts as a partial agonist. 6-SPh-UTP, **16**, 6-SMe-UTP, **17**, 6-OMe-UTP, **18**, and 5-F-UTP, **20**, were not active.

Conformational Analysis of C5/6-Substituted-UTP Derivatives. We expected that an EDG at the C6 position of the uracil base would increase the potency of the UTP analogues **16**−**18** at the $P2Y_{2/4}$-Rs, due to improved H-bonding, $\pi-\pi$, and π−cation interactions. Yet, analogues **16**−**18** showed no activity at the indicated receptors. To rationalize the biochemical results, we attempted to correlate the data with properties of the nucleotides which may affect binding. Thus, we first analyzed the conformation of nucleotides **16**−**22**.

Uracil nucleotides are expected to possess conformational flexibility, due to possible rotations around the glycosidic bond (χ) and pseudorotation of the ribose ring, as well as possible rotations around the C4′−C5′ (γ), C5′−O5′ (β), and O5′−Pα bonds (Figure 6). However, it is well-established that most 5′-nucleotides adopt a predominant conformation in solution (which is nevertheless in equilibrium with other conformations).[28] Thus, it has been shown that a majority of purine and pyrimidine nucleotides favor an *anti* conformation of the base ring with respect to the sugar ring.[29] Likewise, the ribose ring exhibits a puckered conformation in which either the C2′ or C3′ atom is furthest from the plane of the other atoms of the ribose ring, termed the south (*S*) and north (*N*) conformations, respectively.[30] Finally, it has been shown that the ribose exocyclic group exists predominantly in a gauche−gauche (gg) conformation about the C4′−C5′ bond, with the O5′ atom projecting over the furanose ring.

In this study we employed ^1H, ^{13}C, and ^{31}P NMR spectra to analyze the solution conformation of nucleotides **16**−**22**. The chemical shifts and splitting patterns of the nucleotides in D_2O solutions were assigned from ^1H, ^{13}C, and ^{31}P NMR spectra at 600 and 700 MHz (NMR data is summarized in Table 2 in the Supporting Information).

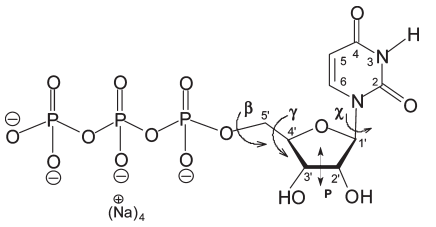

Figure 6. Torsional angles of UTP analogues studied.

Conformation Around the Glycosidic Bond. Pyrimidine nucleotides can adopt two main conformations, *syn* or *anti*, in which the uracil O2 points above or away from the sugar ring. The quantitative determination of the conformation around the glycosidic bond can be obtained by monitoring the vicinal coupling constants $^3J_{C6-H1'}$ and $^3J_{C2-H1'}$, which were extracted from ^{13}C NMR spectra for each nucleotide. We calculated the glycosidic angle χ (O4′−C1′−N1−C2) based on $^3J_{C6-H1'}$ and $^3J_{C2-H1'}$ values as previously described.[31,32] These calculations give several possible χ values. In some cases we had to base our decision on additional conformational evidence. For instance, a cross peak between H-6 and H-2′/3′ in NOESY indicates an *anti* conformation for the nucleotide.[33] A downfield shift of the H-2′ signal, relative to that signal in UTP, is typical of the *syn* conformation.[34] Also, a practical rule for the orientation of the base relative to the ribose was formulated: a value of $^3J_{C2-H1'} < {}^3J_{C6-H1'}$ indicates that χ is in the *anti* conformation, whereas the reverse indicates that χ is in the *syn* conformation.[35] Likewise, for the analysis of the C6-substituted analogues, we relied on previous work by Vorbrüggen[36] for a similar compound (6-methyluridine), which had a preference for the *syn* conformation (probably due to steric hindrance between CH_3 and 5′-CH_2OH).

Ippel et al. reparametrized and generalized the Karplus equations for the glycosidic bond conformation of purine and pyrimidine nucleosides and nucleotides.[35] eqs 1 and 2[35] were used in this study to calculate the glycosidic bond angle χ for nucleotides **16**−**22**. The calculated values of χ angles are shown in Table 2.

Table 2. Conformational Parameters and pK_a Values of Nucleotides **3**,**4**, and **16**−**22**

		C4′−C5′			C5′−O5′							
compound	sugar puckering %	% gg	% tg	% gt	% gg	% tg	% gt	$^3J_{C6-H1'}$	$^3J_{C2-H1'}$	χ	χ_{range}	pK_a (N3−H)[a]
UTP (**3**)	55 (*S*)	n.d.[b]	n.d.	n.d.	n.d.	n.d.	n.d.	4.0	2.0	210	*anti*	9.42
UDP (**4**)	51 (*N*)	84	7	9	64	15	20	n.d.	2.0	217	*anti*	n.m.[c]
6-SPh-UTP (**16**)	70 (*N*)	n.d.	n.d.	n.d.	n.d.	n.d.	n.d.	4.5	6.6	77	*syn*	9.52
6-SMe-UTP (**17**)	75 (*N*)	67	13	20	58	20	22	n.d.	n.d.	n.d.	n.d.	n.m.
6-OMe-UTP (**18**)	68 (*N*)	n.d.	n.d.	n.d.	n.d.	n.d.	n.d.	n.d.	3.5	110	*high-syn*	9.42
5-OMe-UTP (**19**)	66 (*S*)	n.d.	n.d.	n.d.	n.d.	n.d.	n.d.	4.3	n.d.	214	*anti*	9.45
5-F-UTP (**20**)	56 (*S*)	n.d.	n.d.	n.d.	n.d.	n.d.	n.d.	8.1	2.1	210	*anti*	7.85
5-OMe-UDP (**21**)	59 (*S*)	90	6	4	68	25	7	7.8	2.5	240	*anti*	n.m.
5-F-UDP (**22**)	55 (*N*)	n.d.	n.d.	n.d.	n.d.	n.d.	n.d.	n.d.	3.2	200	*anti*	n.m.

[a] The results are the average of two experiments. [b] n.d. = not determined due to second order spectra. [c] n.m. = not measured.

$$^3J_{C6-H1'} = 4.5\cos^2(\chi-60) - 0.6\cos(\chi-60) + 0.1 \quad (1)$$

$$^3J_{C2-H1'} = 4.7\cos^2(\chi-60) + 2.3\cos(\chi-60) + 0.1 \quad (2)$$

The *J*-coupling constants in Table 2 provide strong support for the preferred *anti*-conformer for C5-substituted-UTP analogues. However, the C6-substituted analogues show a preference for the *syn* or *high-syn* conformation (Table 2).

Sugar Puckering. The conformation of the D-ribose ring of nucleotides **16**−**22** was analyzed in terms of a dynamic equilibrium in solution between two favored puckered conformations: a type *N* conformer and a type *S* conformer.[31,32,37] *N* and *S* equilibrium populations were calculated from observed $J_{1'2'}$ and $J_{3'4'}$ couplings, as previously reported.[32] According to this method, the observed vicinal couplings are related to the relative proportion of conformers, given by eqs 3−5:

$$J_{1'2'} = 9.3(1-X_N) + 9.3X_S \quad (3)$$

$$J_{2'3'} = 4.6X_N + 5.3(1-X_N) \quad (4)$$

$$J_{3'4'} = 9.3X_N \quad (5)$$

Using the assigned *J*-coupling constants (Table 2 in Supporting Information) and the above equations, the mole fraction of conformers *S* and *N* for nucleotides **16**−**22** were calculated and the results are summarized in Table 2. For all C6-substituted nucleotides, the predominant ribose puckering is *N*. However, for most of the C5-substituted nucleotides, the predominant ribose puckering is *S*.

Conformations of the Exocyclic CH_2OR Group (R = Phosphate). 1. C4′−C5′ Bond. The coupling constants $J_{4'5'}$ and $J_{4'5''}$ can be interpreted in terms of three classical staggered rotamers, with a preferred gauche−gauche (*gg*) conformation.[32] The mole fractions of each staggered rotamer of C4′−C5′ were calculated from the following expressions (eqs 6−8):

$$\rho_{gg} = [(J_t + J_g) - (J_{4'5'} + J_{4'5''})]/(J_t - J_g) \quad (6)$$

$$\rho_{tg} = (J_{4'5'} - J_g)/(J_t - J_g) \quad (7)$$

$$\rho_{gt} = (J_{4'5''} - J_g)/(J_t - J_g) \quad (8)$$

The coupling constants for pure rotamers were estimated as $J_g = 2.04$ Hz and $J_t = 11.72$ Hz from the appropriate Karplus relation.[32,38] The observed proton signals, labeled H5′ and H5″, refer to downfield and upfield signals, respectively. The results are presented in Table 2. For the 6-SMe-UTP, **17**, and 5-OMe-UDP, **21**, analogues, there is a clear preference for the gg rotamer around the C4′−C5′ bond. For all other analogues, the relative rotamer populations could not be determined, due to second order spectra.

2. C5′−O5′ Bond. Rotamer populations around the C5′−O5′ bond are calculated from ^{31}P−H5′ and ^{31}P−H5″ coupling constants, using procedures analogous to those used for C4′−C5′ (eqs 9−10,11):

$$\rho_{gg} = [(J_t + J_g) - (J_{4'5'} + J_{4'5''})]/(J_t - J_g) \quad (9)$$

$$\rho_{tg} = (J_{4'5'} - J_g)/(J_t - J_g) \quad (10)$$

$$\rho_{gt} = (J_{4'5''} - J_g)/(J_t - J_g) \quad (11)$$

The coupling constants for pure rotamers were estimated as $J_g = 20.9$ Hz and $J_t = 1.8$ Hz.[32] Relative rotamer populations were then calculated from observed $J_{(HCOP)}$ magnitudes (Table 2). Also, in this case, the 6-SMe-UTP, **17**, and 5-OMe-UDP, **21**, analogues exhibited preference for the gg rotamer around the C5′−O5′ bond.

In summary, 5-substituted uridine analogues, for example, **19**, adopted the predominant conformation of UTP, namely, southern, *anti*, and *gg, gg,* for the sugar puckering, χ, α, and β angles, respectively. Yet, 6-substituted uridine analogues, for example, **16**, exhibited an entirely different predominant conformation: a *syn* conformation around the glycosidic angle and preferred northern sugar puckering (Figure 7).

Acid−Base Equilibria—Determination of pK_a Values of Compounds 16−22. The discrepancy between the pharmacological activity expected from our $P2Y_{2/4/6}$-Rs agonists, based on our hypothesis, and the actual biochemical data, encouraged us to evaluate the acid−base equilibria of our analogues, **16**−**22**. pK_a values reflect electronic changes in the uracil ring, which in turn may alter binding interactions with a P2Y-R. The electronic changes may be due to the nature and position of various substituents: an increase in the pK_a value of N3−H can indicate that an EDG at C6 makes O4 less available for resonance with N3−H, therefore, making N3−H less acidic. On the other hand, substitution of an electronegative atom at C5 would exert a negative inductive effect, thus resulting in decreased pK_a values, making N3−H a better H-bond donor.

The pK_a value of the various uridine nucleotide analogues may be related to the strength of H-bonding between the N3−H of each analogue and H-bond acceptors in the P2Y-R. Lower pK_a values, compared to the parent uridine nucleotide, indicate a more polarized N3−H bond, resulting in stronger H-bonds with acceptors in the P2Y-R binding

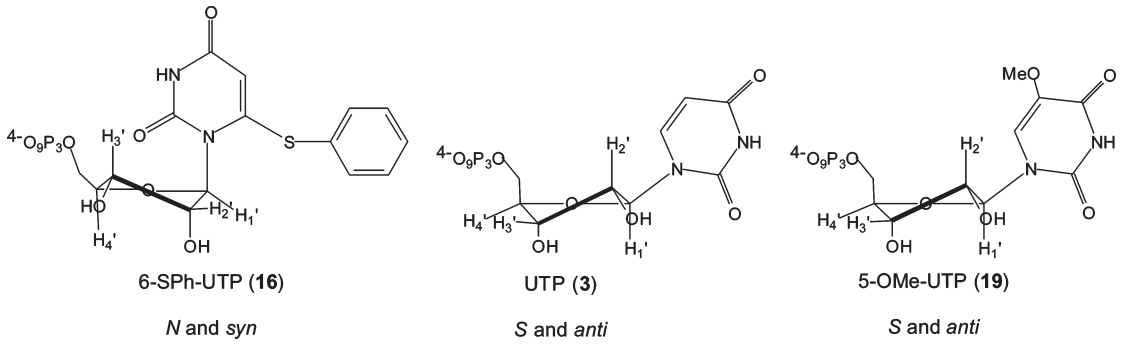

Figure 7. Elucidated conformations of analogues **16** and **19** in solution, compared to that of UTP.

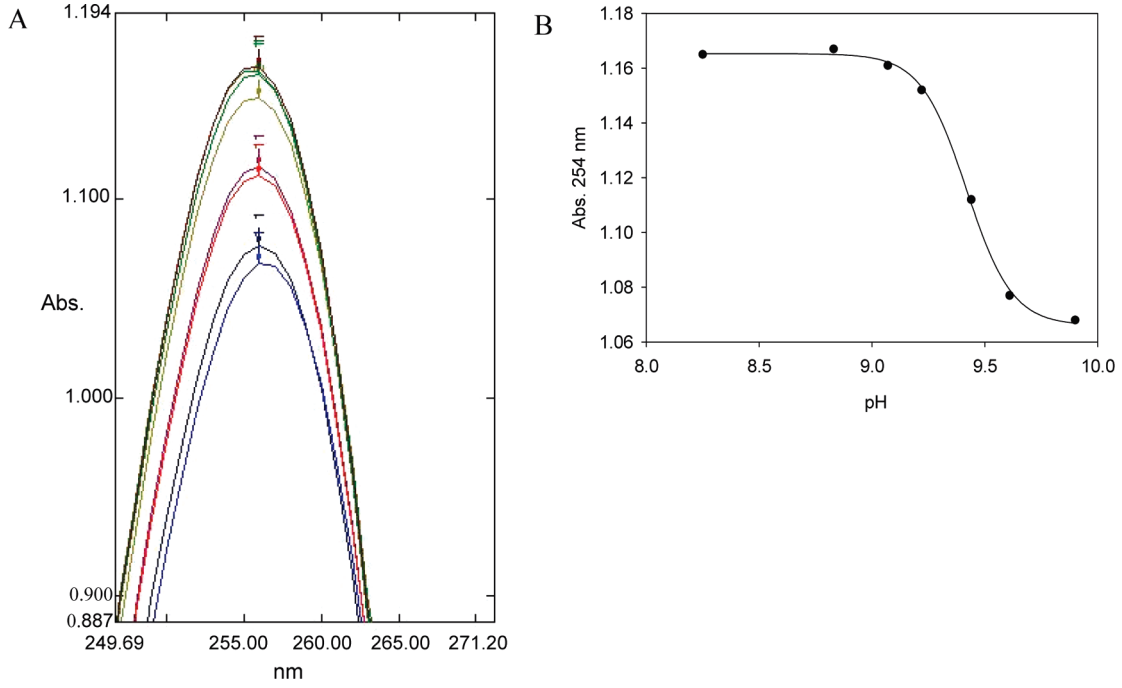

Figure 8. Determination of pK_a of 6-OMe-UTP, **18**. (A) Several solutions of 6-OMe-UTP, **18**, were prepared at different pH values, and their UV absorbance at λ_{max} was measured. (B) The absorbance value plotted vs pH provided a sigmoidal graph from which the pK_a value was calculated.

pocket. Furthermore, deprotonation of the modified uracil, at physiological pH, may result in strong electrostatic interactions between the deprotonated N3 and positively charged residues of the P2Y-R.

Therefore, we have determined the pK_a values of nucleotides **16**−**22** by pH titrations of the analogues, monitored by UV measurements[39] and compared them to that of UTP. Several solutions of each analogue were prepared at different pH values, and their UV absorbance at λ_{max} was measured. Typical UV spectra are shown in Figure 8A. Plotting the absorbance value versus pH provided a sigmoidal graph (Figure 8B). The inflection point (the pK_a value) was extracted from the fitted graph, applying the derivative method, using the following equation:[40]

$$pK_a = pH_1 + (pH_2 - pH_1)\left[\frac{\Delta^2 Abs_1/\Delta pH_1^2}{(\Delta^2 Abs_1/\Delta pH_1^2) + (|\Delta^2 Abs_2/\Delta pH_2^2|)}\right]$$

The pK_a values of analogues **16**−**22** are listed in Table 2. It seems that introduction of an electron-donating group at either C5 or C6 position of the uracil base does not change the pK_a of N3−H of analogues **16**−**19**, compared to UTP. Yet, the 5-flouro substitution, **20**, significantly lowered the pK_a by about 1.5 orders of magnitude (7.85 vs 9.42).

Discussion

Substitutions at Either Position 5 or 6 of Uracil Nucleotides Significantly Affect their Potency at the $P2Y_{2/4/6}$ Receptors. The challenge of finding potent and selective agonists for the $P2Y_{2/4/6}$-Rs, which are more potent than the endogenous ligands, has occupied several research groups over the past decade. So far, only 2−3 such agonists have been found for $P2Y_{2/4/6}$-Rs.[12,14,18]

We addressed this challenge by rational design of uracil nucleotides **16**−**22**, based on our data mining results, and evaluation of the potency and selectivity of the new nucleotides at $P2Y_{2/4/6}$-R. Our major SAR observations here are the following: (A) C6 substitution is not tolerated by the $P2Y_{2/4/6}$ receptors. The design of the C6-substituted analogues was based on the assumption that EDGs at the C6 position, would increase the electron density in the ring and improve $\pi-\pi$ and $\pi-$cation interactions. The uracil ring is

considered to be much less aromatic compared to other heteroatom rings. For example, according to the structural aromaticity index, $\Delta\bar{N}$, it is considered only 45% aromatic, compared to 100% aromaticity attributed to benzene.[41] An EDG at C6 would increase electron density resulting in enhanced aromaticity and improved H-bonding capacity of O4. However, the C6-substituted analogues, **16**−**18**, were found practically inactive or only very weak agonists at all three P2Y-Rs. (B) 5-OMe-UDP is a potent and selective agonist at the $P2Y_6$ receptor. Among the C5-substituted analogues, **19**−**22**, the fluoro-substituted UTP and UDP analogues, **20** and **22**, respectively, were either weak or moderate agonists at the $P2Y_{2/4/6}$-Rs. The 5-OMe analogues, **19** and **21**, on the other hand, were much more promising. 5-OMe-UTP, **19**, was slightly active at the $P2Y_2$-R (EC_{50} 2 μM) and the $P2Y_6$-R (EC_{50} 0.9 μM) with a potency decrease of 20- and 6-fold compared to that of the endogenous ligands for each receptor, **3** and **4**, respectively. Finally, the 5-OMe-UDP, **21**, was proven to be a potent and selective agonist at the $P2Y_6$-R, with an EC_{50} of 0.08 μM, which is about 2-fold more potent than the endogenous agonist **4** (EC_{50} 0.14 μM). The difference between activities of 5-OMe -UTP and −UDP, **19** and **21**, at the $P2Y_2$-R and the $P2Y_6$-R might be due to the preference of each receptor for a different number of phosphate negative charges, four or three, respectively.[12,13] The selectivity and potency of 5-OMe-UDP at $P2Y_6$-R is attributed to both the diphosphate chain and the OMe substitution at C5. (C) 5-F-Substituted uracil nucleotides are active at the $P2Y_{2/4/6}$ receptors. 5-F-UTP, **20**, was found to be a moderate or potent agonist at $P2Y_2$-R and $P2Y_4$-R, EC_{50} 6 and 0.6 μM, respectively. At the $P2Y_6$-R, it showed no activity, demonstrating that recognition by the $P2Y_6$-R requires a diphosphate rather than triphosphate moiety. 5-F-UDP, **22**, acted as a partial agonist at the $P2Y_2$-R, $P2Y_4$-R, and $P2Y_6$-R, with EC_{50} values of 2, 3.5, and 10 μM, respectively. The activity of these analogues might be due to the inductive effect of the fluoro substitution at C5, which makes N3−H a better H-bond donor than in **3** and **4**.

Introduction of Ethers/Thioethers at the 5 or 6 Position of the Uracil Base Does Not Influence the pK_a of N3−H. OR/SR substituents at either the 5 or 6 positions of the uracil base did not influence the pK_a of N3−H. Apparently, the resonance and inductive effects of these substituents on the electronic properties of the uracil base are negligible. However, a fluoro substitution at position 5, **20**, greatly reduced the pK_a of N3−H by about 1.5 log units.[28] This might be one of the reasons for the activity of 5-fluoro-UDP and -UTP at the $P2Y_{2/4/6}$-Rs. Perhaps the greater acidity of N3−H in 5-fluoro-UDP and -UTP, resulting in deprotonation of about 50% of the population at physiological pH, enables electrostatic interactions with positively charged amino acid residues in the $P2Y_{2/4/6}$-Rs binding pocket. These interactions are not possible for the N3−H neutral endogenous ligands, **3** and **4**.

C6-Substituents Have a Significant Influence on the Conformation of UTP Analogues. Because we noticed that the inactivity of **16**−**18** at $P2Y_{2/4/6}$-Rs can not be related to electronic effects on the uracil ring, we considered the steric effects triggered by C6 substituents. The conformational parameters of the nucleotides (sugar puckering, glycosidic angle, etc.) were examined, as they can greatly influence the steric recognition in the P2Y-R binding pocket. The conformational parameters of **3**−**22** were determined by NMR studies and the following conclusions were made.

Table 3. Correlation of Conformation and Activities of Nucleotides **16**−**22**

			agonist activity[a]		
agonist	sugar puckering %	χ_{range}	$P2Y_2$-R	$P2Y_4$-R	$P2Y_6$-R
UTP (**3**)	55(*S*)	*anti*	++[b]	++	−[c]
UDP (**4**)	51(*N*)	*anti*	−	−	++
6-SPh-UTP (**16**)	70(*N*)	*syn*	−	−	−
6-SMe-UTP (**17**)	75(*N*)	n.d.	−	−	−
6-OMe-UTP (**18**)	68(*N*)	*high-syn*	+[d]	−	−
5-OMe-UTP (**19**)	66(*S*)	*anti*	+	−	+
5-F-UTP (**20**)	56(*S*)	*anti*	+	+	−
5-OMe-UDP (**21**)	59(*S*)	*anti*	−	−	++
5-F-UDP (**22**)	55(*N*)	*anti*	+	+	+

[a] Numerical values are detailed in Table 1. [b] Full agonist. [c] Inactive. [d] Partial agonist.

(A). Sugar Puckering is Strongly Dependent on the Substituent at the C5/6 Position of the Uracil. All analogues bearing an electron donating group at position 6 of the uracil group, **16**−**18**, showed a clear preference for the *N* conformer of the ribose ring (Figure 7). The 5-OR-substituted UTP and UDP derivatives, **19** and **21**, respectively, however, showed some preference for the *S* conformer. The 5-F-substituent had a different effect on the UTP and UDP analogues. The 5-F-UTP, **20**, showed some preference for the *S* conformer of the ribose ring, while the 5-F-UDP, **22**, showed some preference for the *N* conformer.

These observations of substituent effect on conformational parameters of the nucleobase, are partially consistent with studies by Uhl et al. showing that an EDG at the 5 position of the uracil base in susbstituted uridine analogues increases the proportion of *N*-type conformations, while EWGs increase the proportion of the *S*-conformer.[42] Our finding that 5-OMe-UDP/UTP, which preferentially adopt the *S* conformation, are active at the $P2Y_6$-R, imply that the *S* sugar pucker is a prerequisite for recognition by $P2Y_6$-R, but not by $P2Y_2$- and $P2Y_4$-Rs (Table 3).

Indeed, an (*N*)-methanocarba ring system in nucleotides locked in an *N* conformation, has been shown to preserve the potency of both adenine and uracil nucleotides at the $P2Y_2$- and $P2Y_4$-Rs.[20] The selectivity of 5-OMe-UDP for the $P2Y_6$-R, induced by the *S* conformation, is supported by molecular modeling studies, indicating that the *S* conformation of the ribose is required for optimal fitting of the UDP sugar moiety in the $P2Y_6$-R binding pocket.[7,19] The *S* ribose conformation positions the phosphate and the nucleobase moieties at the most favorable orientations for binding interactions with the amino acid residues in the TM1, TM3, TM6, and TM7 domains of the $P2Y_6$-R.

(B). Conformation around the Glycosidic Bond is Dependent on Substituents at the C5/6 Position of the Uracil. All χ values calculated for the C5-substituted nucleotides, **19**−**22**, were within the range defined as *anti*, consistent with previous data that pyrimidine analogues substituted at positions other than C2 and C6 exist in a predominantly *anti* conformation.[42] However, the major conformers we determined for the C6-substituted nucleotides, **16** and **17**, were either the *syn* or *high-syn* conformers. Based on the above conformational data, we concluded that steric hindrance, due to interaction between the C6-substituent and C5′, forces the nucleotide into the *syn* or *high-syn* conformations, which are unfavorable by all investigated P2Y-R subreceptors, thus, rendering the C6-substituted uracil analogues inactive (Table 3).

Conclusion

So far, hardly any of the currently known synthetic nucleotides were more potent than the endogenous uracil nucleotides at the $P2Y_{2,4,6}$ receptors. Based on the biochemical activity of uracil nucleotides **16**−**18** at $P2Y_{2,4,6}$-Rs and their conformational analysis, we concluded that C6-substituted UTP derivatives, which adopt the *syn* conformation, are not tolerated by any of these receptors, probably due to steric hindrance. However, a methoxy substituent at position 5 of the uracil ring of UDP has produced almost the most potent and selective agonist at the $P2Y_6$-R currently known. This activity is probably due to the preference of this analogue for the *S* sugar puckering, which is the conformation preferred by the $P2Y_6$-R, but not the $P2Y_2$- or $P2Y_4$-Rs, which require the *N* sugar conformation. 5-OMe-UDP also fulfills the requirements of the $P2Y_{2,4,6}$-Rs of an *anti* conformation around the glycosidic bond. Furthermore, it has the ability of forming an additional H-bonding interaction via the OMe group (H-acceptor). Thus, the uracil 5-OMe-substitution appears to be an important development in the ongoing search for effective $P2Y_6$-R agonists. We plan to apply this finding to produce better agonists for the $P2Y_6$-R. Our results will be published in due course.

Experimental Procedures

Chemistry. General. All air and moisture sensitive reactions were carried out in flame-dried, argon-flushed, two-neck flasks sealed with rubber septa, and the reagents were introduced by syringe. Progress of reactions was monitored by TLC on precoated Merck silica gel plates (60F-254). Visualization was accomplished by UV light. Flash chromatography was carried out on silica gel (Davisil Art. 1000101501). The separation on the automatic column was carried out using an HPFC automated flash purification system (Biotage SP1 separation system (RP)). Compounds were characterized by NMR using Bruker AC-200, DPX-300, or DMX-600 spectrometers. ^{1}H NMR spectra were recorded at 200, 300, or 600 MHz. Chemical shifts are expressed in ppm downfield from Me_4Si (TMS), used as an internal standard. Nucleotides were characterized also by ^{31}P NMR in D_2O, using 85% H_3PO_4 as an external reference on Bruker AC-200 and DMX- 600 spectrometers. High resolution mass spectra were recorded on an AutoSpec Premier (Waters, U.K.) spectrometer by chemical ionization. Nucleotides were analyzed under ESI (electron spray ionization) conditions on a Q-TOF microinstrument (Waters, U.K.). Primary purification of the nucleotides was achieved on a LC (Isco UA-6) system using a Sephadex DEAE-A25 column, swollen in 1 M $NaHCO_3$ at room temperature for 1 day. The resin was washed with deionized water before use. The LC separation was monitored by UV detection at 280 nm. A buffer gradient of NH_4HCO_3 was applied as detailed below. Final purification of the nucleotides was achieved on an HPLC (Merck-Hitachi) system, using a semipreparative reverse-phase column (Gemini 5u C-18 110A, 250 × 10.00 mm, 5 μm, Phenomenex, Torrance, CA). The purity of the nucleotides was evaluated on an analytical reverse-phase column system (Gemini 5u, C-18, 110A, 150 × 4.60 mm, 5 μm, Phenomenex, Torrance, CA), in two solvent systems as described below. The purity of the nucleotides was generally ≥95%. All commercial reagents were used without further purification, unless otherwise noted. 5-Methoxyuridine and 5-F-uridine were purchased from Sigma-Aldrich (St. Louis, U.S.A.). All reactants in moisture sensitive reactions were dried overnight in a vacuum oven. For pK_a measurements, a stainless steel pH electrode with a pH meter (model IQ150, IQ Scientific Instruments, Inc., Carlsbad, Canada) and a UV instrument (UV-2401PC UV−vis recording spectrophotometer, Shimadzu, Kyoto, Japan) were used. All phosphorylation reactions were carried out in flame-dried, argon-flushed, two-neck flasks sealed with rubber septa. Nucleosides were dried in-vacuo overnight. Proton sponge was kept in a desiccator. Phosphorus oxychloride was distilled and kept under nitrogen. The tri-*n*-butylammonium pyrophosphate and tri-*n*-butylammonium phosphate solutions were prepared as described previously.[43] The preparation of the tri--*n*-butylammonium-tri-*n*-octylammonium 5′-monophosphate uridine derivatives was achieved by eluting the uridine nucleotide derivative (as obtained after LC separation) through an activated Dowex-H^+ form using deionized water. The resulting solution dropped to an ice-cooled EtOH solution containing 1 equiv tri-*n*-octylamine and 1 equiv tri-*n*-butylamine. Nucleosides **23**−**27** were prepared according to previously published procedures.[21−26]

6 Methoxy-uridine, 25. To a nitrogen-flushed round-bottom flask containing compound **23** (102.9 mg, 0.292 mmol), a solution of NaOMe in freshly distilled dry MeOH (3.7 mL, 11.52 mmol, 39 equiv) was added. The resulting clear solution was stirred at room temperature. TLC of samples that were neutralized with 10% HCl, on a silica gel plate ($CHCl_3$/MeOH 7:3) showed the presence of a more polar product (R_f 0.31). After 2.5 days, the reaction mixture was quenched with a few drops of 10% HCl, and the resulting solution was freeze-dried. The product was purified utilizing silica gel column chromatography ($CHCl_3$/MeOH 95:5 to 8:2; 34.4 mg, 43%). ^{1}H NMR (600 MHz) δ CD_3OD: 6.12 (d, J = 3.3 Hz, 1H, H-1′), 5.15 (s, 1H, H-5), 4.57 (dd, J = 6.2, 3.3 Hz, 1H, H-2′), 4.24 (t, J = 6.2 Hz, 1H, H-3′), 3.93 (s, 3H, OCH_3), 3.81 (m, 2H, H-4′,H-5′), 3.64 (dd, J = 12.6, 5.9 Hz, 1H, H-5″) ppm. HR MALDI (positive): Calcd for $C_{10}H_{14}N_2Na_1O_7$, 297.069; found, 297.069.

Typical Procedure for the Preparation of Uridine Nucleoside 5′-Triphosphate Derivatives. A solution of 6-methoxy-uridine, **25** (38.2 mg, 0.139 mmol) in dry trimethyl phosphate (0.9 mL) was cooled to 0 °C; then proton sponge (59.7 mg, 0.278 mmol, 2 equiv) was added. After 20 min, the flask was put in an ethylene glycol−dry ice bath at a temperature of −15 °C and distilled phosphorus oxychloride (25.6 μL, 0.28 mmol, 2 equiv) was then added dropwise. A clear purple solution was obtained. Stirring continued for 3.5 h at −15 °C. TLC on a silica gel plate ($CHCl_3$/MeOH 7:3) indicated the disappearance of the starting material and the formation of a polar product. A mixture of Bu_3N (0.13 mL, 0.55 mmol, 4 equiv) and 1 M $(Bu_3NH^+)_2P_2O_7H_2^{-2}$ in DMF (0.83 mL, 0.83 mmol, 6 equiv) was added at once. After 6 min, a 1 M TEAB solution (pH = 8; 3.4 mL) was added, and the clear solution was then stirred at room temperature for 45 min. TLC on a silica gel plate (isopropanol/25% NH_4OH/H_2O 11:2:7) indicated the presence of more polar products (R_f = 0.38, 0.31). The solution was freeze-dried overnight. The semisolid obtained after freeze-drying was chromatographed on an activated Sephadex DEAE-A25 column. The resin was washed with deionized water and loaded with the crude reaction residue dissolved in a minimal volume of water. The separation was monitored by UV detection at 280 nm. A buffer gradient of 200 mL water to 200 mL 0.2 M NH_4HCO_3 was used, followed by a buffer gradient of 300 mL 0.2 M NH_4HCO_3 to 300 mL 0.4 M NH_4HCO_3. The relevant fractions were pooled and freeze-dried three times to yield a white solid. Final purification was carried out by HPLC, using a semipreparative reverse-phase column. The purity of the nucleotides was evaluated on an analytical reverse-phase column system in two solvent systems, as described below. The products, obtained as triethylammonium salts, were generally ≥95% pure. Finally, the products (dissolved in water) were passed through a Dowex 50WX8−200 sodium form ion-exchange resin column and eluted with deionized water to obtain the corresponding sodium salts after freeze-drying.

6-SPh-UTP, **16**, was obtained from 6-SPh-uridine, **23** (90.9 mg, 0.258 mmol) in a 63% (103.9 mg) yield after LC separation. Final separation was achieved by applying a linear gradient of TEAA/CH_3CN 85:15 to 78:22 in 30 min (5 mL/min): t_R 8.63 min.

Purity data obtained on an analytical column: t_R 7.19 min (91% purity) using solvent system I (80:20 to 70:30 TEAA/CH_3CN over 10 min, 1 mL/min); t_R 2.27 min (76% purity) using solvent system II (100:0 to 95:5 of 0.01 M KH_2PO_4 (pH = 4.6)/MeOH over 10 min, 1 mL/min). ^{1}H NMR (600 MHz, D_2O) δ: 7.56−7.66 (m, 5H, Ph), 6.10 (d, J = 3.2, 1H, H-1′), 5.14 (s, 1H, H-5), 4.89 (dd, J = 6.5, 3.2 Hz, 1H, H-2′), 4.52 (t, J = 6.9 Hz, 1H, H-3′), 4.28 (m, 1H, H5′), 4.13−4.18 (m, 2H, H-4′, H-5″) ppm. ^{31}P NMR (240 MHz, D_2O) δ: −9.07 (d, J = 19.0 Hz, P_γ), −10.36 (d, J = 19.0 Hz, P_α), −22.03 (t, J = 19.0 Hz, P_β) ppm. HR MALDI (negative): Calcd for $C_{15}H_{18}N_2Na_2O_{15}P_3S_1$, 639.943; found, 639.948. UV (H_2O, pH 7) λ_{max}: 284 nm.

6-SMe-UTP, **17**, was obtained from 6-SMe-uridine, **24** (102.8 mg, 0.39 mmol) in a 3% (7.8 mg) yield (after HPLC). Final separation was achieved by applying a linear gradient of TEAA/CH_3CN 95:5 to 85:15 in 20 min (5 mL/min): t_R 8.45 min. Purity data obtained on an analytical column: t_R 7.57 min (88% purity) using solvent system I (80:20 to 70:30 TEAA/CH_3CN over 10 min, 1 mL/min); t_R 2.33 min (89% purity) using solvent system II (95:5 to 90:10 of 0.01 M KH_2PO_4 (pH = 4.6)/CH_3CN over 10 min, 1 mL/min). ^{1}H NMR (600 MHz, D_2O) δ: 5.99 (d, J = 3.5, 1H, H-1′), 5.63 (s, 1H, H-5), 4.83 (dd, J = 6.8, 3.5 Hz, 1H, H-2′), 4.51 (t, J = 6.9 Hz, 1H, H-3′), 4.26 (m, 1H, H5′), 4.12−4.14 (m, 2H, H-4′,H-5″), 2.55 (s, 3H, CH_3) ppm. ^{31}P NMR (D_2O) δ: −5.35 (d, J = 21.3 Hz, P_γ), −10.02 (d, J = 18.8 Hz, P_α), −21.04 (t, J = 19.5 Hz, P_β) ppm. MS: MALDI (positive) 575 $[M - H^+ + 2Na^+]^+$.

6-OMe-UTP, **18**, was obtained from 6-OMe-uridine, **25** (38.2 mg, 0.14 mmol) in a 35% (39.9 mg) yield (after HPLC). Final separation was achieved by applying a linear gradient of TEAA/CH_3CN 98:2 to 90:10 in 20 min (5 mL/min): t_R 8.83 min. Purity data obtained on an analytical column: t_R 4.53 min (97% purity) using solvent system I (98:2 to 90:10 TEAA/CH_3CN over 20 min, 1 mL/min); t_R 2.31 min (94% purity) using solvent system II (100:0 to 95:5 of 0.01 M KH_2PO_4 (pH = 4.6)/MeOH over 10 min, 1 mL/min). ^{1}H NMR (600 MHz, D_2O) δ: 6.21 (bs, 1H, H-1′), 5.28 (s, 1H, H-5), 4.67 (bs, 1H, H-2′), 4.46 (t, J = 7 Hz, 1H, H-3′), 4.23 (ddd, J = 11.9, 5.6, 3.3 Hz, 1H, H-5′), 4.19 (m, 1H, H5″), 4.10 (m, 1H, H4′), 3.99 (s, 3H, CH_3) ppm. ^{31}P NMR (240 MHz, D_2O) δ: −5.54 (d, J = 19 Hz, P_γ), −10.04 (d, J = 19.4 Hz, P_α), −21.09 (t, J = 19.2 Hz, P_β) ppm. HR MALDI (negative): Calcd for $C_{10}H_{16}N_2O_{16}P_3$, 512.971; found, 512.975. UV (H_2O, pH 7) λ_{max}: 242 nm.

5-OMe-UTP, **19**, was obtained from 5-OMe-uridine, **26** (50 mg, 0.18 mmol) in an 11% (11.2 mg) yield (after LC). Final separation was achieved by applying a linear gradient of TEAA/CH_3CN 95:5 to 85:15 in 20 min (4.5 mL/min): t_R 4.83 min. Purity data obtained on an analytical column: t_R 4.21 min (89% purity) using solvent system I (100:0 to 85:15 TEAA/CH_3CN over 20 min, 1 mL/min); t_R 2.64 min (89% purity) using solvent system II (100:0 to 95:5 of 0.01 M KH_2PO_4 (pH = 4.6)/MeOH over 10 min, 1 mL/min). ^{1}H NMR (600 MHz, D_2O) δ: 7.38 (s, 1H, H-6), 6.03 (d, J = 6.1, 1H, H-1′), 4.50 (dd, J = 5.4, 3.1 Hz, 1H, H-3′), 4.46 (t, J = 5.8 Hz, 1H, H-2′), 4.26−4.31 (m, 2H, H-3′, H-5′), 4.18 (m, 1H, H5″), 3.80 (s, 3H, CH_3) ppm. ^{31}P NMR (240 MHz, D_2O) δ: −5.31 (d, J = 19.8 Hz, P_γ), −10.60 (d, J = 19.7 Hz, P_α), −21.10 (t, J = 19.6 Hz, P_β) ppm. HR MALDI (negative): Calcd for $C_{10}H_{16}N_2O_{16}P_3$, 512.971; found, 512.970. UV (H_2O, pH 7) λ_{max}: 278 nm.

5-F-UTP, **20**, was obtained from 5-F-uridine, **27** (97 mg, 0.37 mmol) in a 26.1% (77.9 mg) yield (after HPLC). Final separation was achieved by applying a linear gradient of TEAA/CH_3CN 98:2 to 90.5:9.5 in 12 min (5 mL/min): t_R 7.07 min. Purity data obtained on an analytical column: t_R 4.34 min (94% purity) using solvent system I (98:2 to 90:10 TEAA/CH_3CN over 20 min, 1 mL/min). t_R: 6.18 min (93% purity) using solvent system II (100:0 to 96:4 of 0.01 M KH_2PO_4 (pH = 4.6): CH_3CN over 20 min, 1 mL/min). ^{1}H NMR (600 MHz, D_2O) δ: 8.04 (d, J = 6.4 Hz, 1H, H-6), 5.89 (dd, J = 5.2, 1.6 Hz, 1H, H-1′), 4.34 (t, J = 4.9 Hz, 1H, H-3′), 4.30 (t, J = 5.4 Hz, 1H, H-2′), 4.20 (quint, J = 2.3 Hz, 1H, H-4′), 4.17−4.18 (m, 2H, H5′, H5″) ppm. ^{31}P NMR (240 MHz, D_2O) δ: −8.41 (d, J = 19.0 Hz, P_γ), −10.66 (d, J = 20.2 Hz, P_α), −21.80 (t, J = 19.4 Hz, P_β) ppm. HR MALDI (negative): Calcd for $C_9H_{12}F_1N_2O_{15}P_3$, 499.943; found, 499.940. UV (H_2O, pH 7) λ_{max}: 270 nm.

Typical Procedure for the Preparation of Uridine Nucleoside 5′-Monophosphate Derivatives. A solution of 5-fluoro-uridine, **27** (95.7 mg, 0.365 mmol) in dry trimethyl phosphate (1.5 mL) was cooled to −15 °C using an ethylene glycol−dry ice bath; then proton sponge (234 mg, 1.01 mmol, 3 equiv) was added. After 20 min, distilled phosphorus oxychloride (60 μL, 0. 73 mmol, 2 equiv) was added dropwise. Stirring continued for 3 h at −15 °C. TLC on a silica gel plate (isopropanol/25% NH_4OH/H_2O 11:2:7) indicated the disappearance of the starting material and the formation of a more polar product. TEAB solution (1 M, 8 mL, pH 8) was then added until neutralization, and the clear solution was stirred at room temperature for 45 min. The solution was freeze-dried overnight. The semisolid obtained after freeze-drying was chromatographed on an activated Sephadex DEAE-A25 column. The resin was washed with deionized water and loaded with the crude reaction residue dissolved in a minimal volume of water. The separation was monitored by UV detection at 280 nm. A buffer gradient of 500 mL of water to 500 mL of 0.2 M NH_4HCO_3 was used. The relevant fraction was collected and freeze-dried three times until a constant weight was obtained to yield the product as a white solid (122.5 mg, 81%).

Typical Procedure for the Preparation of Uridine Nucleoside 5′-Diphosphate Derivatives. A solution of 5-fluoro-5′-monophosphate-uridine *n*-butylammonium-*n*-octylammonium salt in dry DMF (4 mL) was added to a two-neck round-bottom flask containing carbonyldiimidazole (24 mg, 1.48 mmol, 5 equiv). TLC on a silica gel plate (isopropanol/25% NH_4OH/H_2O 11:2:7), indicated the disappearance of the starting material (R_f 0.32) and the formation of a less polar product (R_f 0.63). After 3 h, distilled MeOH (0.1 mL) was added. A precipitate was formed and the mixture was stirred for 5 min. Then, a solution of 1 M $(Bu_3NH^+)_2PO_4H^{2-}$ in DMF (1.18 mL, 1.18 mmol, 4 equiv) was added, and the turbid solution was stirred at RT for 2 days. TLC indicated the appearance of a new polar product (R_f 0.32) and the solution was freeze-dried overnight. The semisolid obtained after freeze-drying was chromatographed on an activated Sephadex DEAE-A25 column. The resin was washed with deionized water and loaded with the crude reaction residue dissolved in a minimal volume of water. The separation was monitored by UV detection (ISCO, UA-6) at 280 nm. A buffer gradient of 400 mL of water to 400 mL of 0.25 M NH_4HCO_3 was used. The different fractions were pooled and freeze-dried three times to yield a white solid. Final purification was carried out on an HPLC system, using a semipreparative reverse-phase column. The purity of the nucleotides was evaluated on an analytical reverse-phase column system, in two solvent systems as described below. The products, obtained as triethylammonium salts, were generally ≥95% pure. Finally, aqueous solutions of the products were passed through a sodium form Dowex 50WX8-200 ion-exchange resin column and the products were eluted with deionized water to obtain the corresponding sodium salts after freeze-drying.

5-OMe-UDP, **21**, was obtained from 5-OMe-uridine, **26** (30.1 mg, 0.08 mmol) in a 27% (13.3 mg) yield (after HPLC). Final separation was achieved by applying a linear gradient of TEAA/CH_3CN 98:2 to 93:7 in 12.5 min (5 mL/min): t_R 6.74 min. Purity data obtained on an analytical column: t_R 3.33 min (99% purity) using solvent system I (98:2 to 90:10 TEAA/CH_3CN over 20 min, 1 mL/min). t_R 2.00 min (96% purity) using solvent system II (100:0 to 96:4 of 0.01 M KH_2PO_4 (pH = 4.6): CH_3CN over 20 min, 1 mL/min). ^{1}H NMR (600 MHz, D_2O) δ: 7.30 (s, 1H, H-6), 5.95 (d, J = 5.5, 1H, H-1′), 4.35−4.37 (m, 2H, H-3′, H2′), 4.22 (quint, J = 2.5 Hz, 1H, H-4′), 4.15−4.18 (ddd, J = 12.0, 6.5, 2.6 Hz, 1H, H-5′), 4.11−4.13 (ddd, J = 12.0, 3.2, 2.4

Hz, 1H, H-5″), 3.73 (s, 3H, CH_3) ppm. ^{31}P NMR (240 MHz, D_2O) δ: −8.82 (d, J = 20.8 Hz, P_β), −10.68 (d, J = 20.8 Hz, P_α) ppm. HR MALDI (negative): Calcd for $C_{10}H_{15}N_2O_{13}P_2$, 433.004; found, 433.003. UV (H_2O, pH 7) λ_{max}: 278 nm.

5-F-UDP, **22**, was obtained from 5-F-uridine, **27** (122.5 mg, 0.29 mmol) in a 16% (30 mg) yield (after HPLC). Final separation was achieved by applying a linear gradient of TEAA/CH_3CN 98:2 to 93.9:6.1 in 10.2 min (5 mL/min): t_R 5.97 min. Purity data obtained on an analytical column: t_R 6.67 min (95% purity) using solvent system I (100:0 to 96:4 TEAA/CH_3CN over 20 min, 1 mL/min). t_R 1.96 min (92% purity) using solvent system II (100:0 to 96:4 of 0.01 M KH_2PO_4 (pH = 4.6): CH_3CN over 10 min, 1 mL/min). ^{1}H NMR (600 MHz, D_2O) δ: 8.06 (d, J = 6.4 Hz, 1H, H-6), 5.86 (dd, J = 4.6, 1.6 Hz, 1H, H-1′), 4.34 (t, J = 5.3 Hz, 1H, H-3′), 4.28 (t, J = 4.8 Hz, 1H, H-2′), 4.18 (quint, J = 2.5 Hz, 1H, H-4′), 4.14−4.17 (m, 2H, H5′, H5″) ppm. ^{31}P NMR (240 MHz, D_2O) δ: −7.00 (d, J = 22.1 Hz, P_β), −10.39 (d, J = 22.1 Hz, P_α) ppm. HR MALDI (negative): Calcd for $C_9H_{12}F_1N_2O_{12}P_2$, 420.984; found, 420.980. UV (H_2O, pH 7) λ_{max}: 270 nm.

pK_a Measurements. Typical Procedure. A total of 14 solutions of 100 μM 6-OMe-UTP, **18**, at a constant 1 M ionic strength (using 1 M $NaClO_4$ in HPLC-grade water) were prepared and titrated by 0.01−1 M NaOH to pH ∼7 to ∼12. The controls used for UV measurements were 1 M $NaClO_4$ solutions in HPLC-grade water, adjusted to the same pH as the sample. The absorbances of the samples at λ_{max} 262 nm provided a sigmoidal graph, and a fitted graph using Sigma-Plot software (SPSS Inc., Chicago, IL) was obtained. The pK_a was extracted from the fitted graph using the second derivative method.

Data Mining. Generation of Data Set. Protein structures with bound uracil/uridine were identified using the ligand-based search option available from the PDB web site (http://pdbbeta.rcsb.org/pdb/). A nonredundant set of high-resolution structures was extracted using the PISCES sequence-culling server (http://dunbrack.fccc.edu/PISCES.php). The PISCES server uses a combination of structure alignments at low sequence identity and sequence alignments using PSI-BLAST at high sequence identity and has been shown to produce larger sets of nonredundant structures than other culling methods.[44] A chain-based culling was used with a maximum sequence identity of 30% and a maximum resolution of 3.0 Å. Default settings were maintained for all other parameters. Complexes in which the uracil moiety was largely exposed to solvent, lacking interactions with the protein were eliminated from the analysis. The pruned set contained 44 structures with resolution under 2.6 Å (Table 1, Supporting Information).

Identification of Protein−Ligand Interactions. Interactions involved in uracil/ribose recognition were identified in each of the remaining structures by visual inspection of all amino acids within a 7.0 Å distance from the ligand. Putative hydrogen bonds were defined using a distance cutoff of 3.5 Å between donor and acceptor atoms and in consideration of plausible bond angles between donor atom and the attached hydrogen missing from the structure.

Evaluation of Activity of Analogues 16−22 at $P2Y_{2/4/6}$-Rs. Cell Culture and Transfection. GFP (green fluorescent protein) constructs of human $P2Y_2$-R, $P2Y_4$-R, and $P2Y_6$-R were expressed in 1321N1 astrocytoma cells, which lack endogenous expression of P2X- and P2Y-Rs. The respective cDNA of the receptor gene was cloned into a pEGFPN1 vector, and after transfection, using FuGENE 6 Transfection Reagent (Roche Molecular Biochemicals, Mannheim, Germany), cells were selected with 0.5 mg/mL G418 (geneticine; Merck Chemicals, Darmstadt, Germany) and grown in Dulbecco's modified Eagles' medium (DMEM) supplemented with 10% fetal calf serum (FCS), 100 U/mL penicillin, and 100 U/mL streptomycin at 37 °C and 5% CO_2. The functional expression of the receptor was confirmed via GFP fluorescence and change of $[Ca^{2+}]_i$ after stimulation with the respective standard receptor agonists.

Calcium Measurements. The 1321N1 astrocytoma cells, transfected with the respective plasmid for P2YR-GFP expression plated on coverslips (22 mm diameter) and grown to approximately 80% density, were incubated with 2 μM fura 2/AM and 0.02% pluronic acid in Na-HBS buffer (Hepes buffered saline: 145 mM NaCl, 5.4 mM KCl, 1.8 mM $CaCl_2$, 1 mM $MgCl_2$, 25 mM glucose, 20 mM Hepes/Tris, pH 7.4) for 30 min at 37 °C. The cells were superfused (1 mL/min, 37 °C) with different concentrations of the agonist, and the change in $[Ca^{2+}]_i$ was measured by monitoring the respective emission intensity at 510 nm after 340 and 380 nm excitations.[45] Concentration−response data were analyzed with the SigmaPlot software (SPSS Inc., Chicago, IL) using the ratio of the fluorescence intensities with 340 and 380 nm excitation.[46,47]

Supporting Information Available: Details about the uracil/uridine derivatives and binding proteins inspected in the data mining process, and information about chemical shifts and J coupling of all final compounds. This material is available free of charge via the Internet at http://pubs.acs.org.

References

(1) Abbracchio, M. P.; Burnstock, G.; Boeynaems, J.; Barnard, E. A.; Boyer, J. L.; Kennedy, C.; E., K. G.; Fumagalli, M.; Gachet, C.; Jacobson, K. A.; Weisman, G. A. International Union of Pharmacology LVIII: Update on the P2Y G protein-coupled nucleotide receptors: from molecular mechanisms and pathophysiology to therapy. *Pharmacol. Rev.* **2006**, *58*, 281–341.

(2) Yerxa, B. R.; Sabater, J. R.; Davis, C. W.; Stutts, M. J.; Lang-Furr, M.; Picher, M.; Jones, A. C.; Cowlen, M.; Dougherty, R.; Boyer, J.; Abraham, W. M.; Boucher, R. C. Pharmacology of INS37217 [P1-(uridine 5′)-P4-(2′-deoxycytidine 5′)tetraphosphate, tetrasodium salt], a next-generation P2Y2 receptor agonist for the treatment of cystic fibrosis. *J. Pharmacol. Exp. Ther.* **2002**, *302*, 871–880.

(3) Pintor, J.; Peral, A.; Pelaez, T.; Carracedo, G.; Bautista, A.; Hoyle, C. H. V. Nucleotides and dinucleotides in ocular physiology: New possibilities of nucleotides as therapeutic agents in the eye. *Drug Dev. Res.* **2003**, *59*, 136–145.

(4) Schnurr, M.; Toy, T.; Stoitzner, P.; Cameron, P.; Shin, A.; Beecroft, T.; Davis, I. D.; Cebon, J.; Maraskovsky, E. ATP gradients inhibit the migratory capacity of specific human dendritic cell types: Implications for P2Y11 receptor signaling. *Blood* **2003**, *102*, 613–620.

(5) Agteresch, H. J.; van Rooijen, M. H. C.; van den Berg, J. W. O.; Minderman-Voortman, G. J.; Wilson, J. H. P.; Dagnelie, P. C. Growth inhibition of lung cancer cells by adenosine 5′-triphosphate. *Drug Dev. Res.* **2003**, *60*, 196–203.

(6) Robaye, B.; Ghanem, E.; Wilkin, F.; Fokan, D.; Van Driessche, W.; Schurmans, S.; Boeynaems, J.-M.; Beauwens, R. Loss of nucleotide regulation of epithelial chloride transport in the jejunum of P2Y4-null mice. *Mol. Pharmacol.* **2003**, *63*, 777–783.

(7) Besada, P.; Shin, D. H.; Costanzi, S.; Ko, H.; Mathe, C.; Gagneron, J.; Gosselin, G.; Maddileti, S.; Harden, T. K.; Jacobson, K. A. Structure−activity relationships of uridine 5′-diphosphate analogues at the human P2Y6 receptor. *J. Med. Chem.* **2006**, *49*, 5532–5543.

(8) Somers, G. R.; Hammet, F. M. A.; Trute, L.; Southey, M. C.; Venter, D. J. Expression of the P2Y6 purinergic receptor in human T cells infiltrating inflammatory bowel disease. *Lab. Invest.* **1998**, *78*, 1375–1383.

(9) Brunschweiger, A.; Muller, C. E. P2 receptors activated by uracil nucleotides—an update. *Curr. Med. Chem.* **2006**, *13*, 289–312.

(10) El-Tayeb, A.; Qi, A.; Muller, C. E. Synthesis and structure-activity relationships of uracil nucleotide derivatives and analogues as agonists at human P2Y2, P2Y4, and P2Y6 receptors. *J. Med. Chem.* **2006**, *49*, 7076–7087.

(11) Jacobson, K. A.; Costanzi, S.; Ivanov, A. A.; Tchilibon, S.; Besada, P.; Gao, Z.-G.; Maddileti, S.; Harden, T. K. Structure activity and molecular modeling analyses of ribose- and base-modified uridine 5′-triphosphate analogues at the human P2Y2 and P2Y4 receptors. *Biochem. Pharmacol.* **2006**, *71*, 540–549.

(12) Jacobson, K. A.; Ivanov, A. A.; Castro, S.; Harden, T. K.; Ko, H. Development of selective agonists and antagonists of P2Y receptors. *Purinergic Signalling* **2009**, *5*, 75–89.

(13) Shaver, S. R.; Rideout, J. L.; Pendergast, W.; Douglass, J. G.; Brown, E. G.; Boyer, J. L.; Patel, R. I.; Redick, C. C.; Jones, A. C.;

Picher, M.; Yerxa, B. R. Structure−activity relationships of dinucleotides: Potent and selective agonists of P2Y receptors. *Purinergic Signalling* **2005**, *1*, 183–191.
(14) Ivanov, A. A.; Ko, H.; Cosyn, L.; Maddileti, S.; Besada, P.; Fricks, I.; Costanzi, S.; Harden, T. K.; Van Calenbergh, S.; Jacobson, K. A. Molecular modeling of the human P2Y2 receptor and design of a selective agonist, 2′-amino-2′-deoxy-2-thiouridine 5′-triphosphate. *J. Med. Chem.* **2007**, *50*, 1166–1176.
(15) Knoblauch, B. H. A.; Muller, C. E.; Jarlebark, L.; Lawoko, G.; Kottke, T.; Wikstrom, M. A.; Heilbronn, E. 5-Substituted UTP derivatives as P2Y2 receptor agonists. *Eur. J. Med. Chem.* **1999**, *34*, 809–824.
(16) Communi, D.; Parmentier, M.; Boeynaems, J.-M. Cloning, functional expression and tissue distribution of the human P2Y6 receptor. *Biochem. Biophys. Res. Commun.* **1996**, *222*, 303–308.
(17) Nicholas, R. A.; Watt, W. C.; Lazarowski, E. R.; Li, Q.; Harden, T. K. Uridine nucleotide selectivity of three phospholipase C-activating P2 receptors: identification of a UDP-selective, a UTP-selective, and an ATP- and UTP-specific receptor. *Mol. Pharmacol.* **1996**, *50*, 224–229.
(18) Korcok, J.; Raimundo, L. N.; Du, X.; Sims, S. M.; Dixon, S. J. P2Y6 nucleotide receptors activate NF-kB and increase survival of osteoclasts. *J. Biol. Chem.* **2005**, *280*, 16909–16915.
(19) Costanzi, S.; Joshi, B. V.; Maddileti, S.; Mamedova, L.; Gonzalez-Moa, M. J.; Marquez, V. E.; Harden, T. K.; Jacobson, K. A. Human P2Y6 receptor: molecular modeling leads to the rational design of a novel agonist based on a unique conformational preference. *J. Med. Chem.* **2005**, *48*, 8108–8111.
(20) Kim, H. S.; Ravi, R. G.; Marquez, V. E.; Maddileti, S.; Wihlborg, A.-K.; Erlinge, D.; Malmsjoe, M.; Boyer, J. L.; Harden, T. K.; Jacobson, K. A. Methanocarba modification of uracil and adenine nucleotides: high potency of northern ring conformation at P2Y1, P2Y2, P2Y4, and P2Y11 but not P2Y6 receptors. *J. Med. Chem.* **2002**, *45*, 208–218.
(21) Hayakawa, H.; Tanaka, H.; Miyasaka, T. Lithiation of 5,6-dihydrouridine: a new route to 5-substituted uridines. *Tetrahedron* **1985**, *41*, 1675–1683.
(22) Hayakawa, H.; Tanaka, H.; Obi, K.; Itoh, M.; Miyasaka, T. A simple and general entry to 5-substituted uridines based on regioselective lithiation controlled by a protecting group in the sugar moiety. *Tetrahedron Lett.* **1987**, *28*, 87–90.
(23) Hayakawa, H.; Tanaka, H.; Maruyama, Y.; Miyasaka, T. Regioselectivity in the lithiation of uridine. Effect of the sugar protecting groups. *Chem. Lett.* **1985**, 1401–1404.
(24) Evans, M. E.; Parrish, F. W.; Long, L., Jr. Acetal exchange reactions. *Carbohydr. Res.* **1967**, *3*, 453–462.
(25) Tanaka, H.; Hayakawa, H.; Miyasaka, T. Umpolung of reactivity at the C-6 position of uridine: a simple and general method for 6-substituted uridines. *Tetrahedron* **1982**, *38*, 2635–2642.
(26) Tanaka, H.; Iijima, S.; Matsuda, A.; Hayakawa, H.; Miyasaka, T.; Ueda, T. The reaction of 6-phenylthiouridine with sulfur nucleophiles: a simple and regiospecific preparation of 6-alkylthiouridines and 6-alkylthiouridylic acids. *Chem. Pharm. Bull.* **1983**, *31*, 1222–1227.
(27) Halbfinger, E.; Major, D. T.; Ritzmann, M.; Ubl, J.; Reiser, G.; Boyer, J. L.; Harden, K. T.; Fischer, B. Molecular recognition of modified adenine nucleotides by the P2Y1-receptor. 1. A synthetic, biochemical, and NMR approach. *J. Med. Chem.* **1999**, *42*, 5325–5337.
(28) Saenger, W. *Principles of Nucleic Acid Structure*; Springer-Verlag: New York, 1984; pp 107−110.
(29) Donohue, J.; Trueblood, K. N. Base pairing in DNA. *J. Mol. Biol.* **1960**, *2*, 363–371.
(30) Sundaralingam, M. Stereochemistry of nucleic acids and their constituents. IV. Allowed and preferred conformations of nucleosides, nucleoside mono-, di-, tri-, tetraphosphates, nucleic acids, and polynucleotides. *Biopolymers* **1969**, *7*, 821–860.
(31) Altona, C.; Sundaralingam, M. Conformational analysis of the sugar ring in nucleosides and nucleotides. Improved method for the interpretation of proton magnetic resonance coupling constants. *J. Am. Chem. Soc.* **1973**, *95*, 2333–2344.
(32) Davies, D. B.; Danyluk, S. S. Nuclear magnetic resonance studies of 5′-ribo- and deoxyribonucleotide structures in solution. *Biochemistry* **1974**, *13*, 4417–4434.
(33) Prado, F. R.; Giessner-Prettre, C.; Pullman, B. On the conformational dependence of the proton chemical shifts in nucleosides and nucleotides. III. Proton chemical shifts of 5′-nucleotides as a function of different conformational parameters. *J. Theor. Biol.* **1978**, *74*, 259–277.
(34) Schweizer, M. P.; Banta, E. B.; Witkowski, J. T.; Robins, R. K. Determination of pyrimidine nucleoside syn,anti conformational preference in solution by proton and carbon-13 nuclear magnetic resonance. *J. Am. Chem. Soc.* **1973**, *95*, 3770–3778.
(35) Ippel, J. H.; Wijmenga, S. S.; de Jong, R.; Heus, H. A.; Hilbers, C. W.; de Vroom, E.; van der Marel, G. A.; van Boom, J. H. Heteronuclear scalar couplings in the bases and sugar rings of nucleic acids: their determination and application in assignment and conformational analysis. *Magn. Reson. Chem.* **1996**, *34*, S156–S176.
(36) Suck, D.; Saenger, W.; Vorbrüggen, H. Conformation of 6-methyluridine, a pyrimidine nucleoside in the syn conformation. *Nature* **1972**, *235*, 333–334.
(37) Altona, C.; Sundaralingam, M. Conformational analysis of the sugar ring in nucleosides and nucleotides. A new description using the concept of pseudorotation. *J. Am. Chem. Soc.* **1972**, *94*, 8205–8212.
(38) Blackburn, B. J.; Grey, A. A.; Smith, I. C. P.; Hruska, F. E. Determination of the molecular conformation of uridine in aqueous solution by proton magnetic resonance spectroscopy. Comparison with β-pseudouridine. *Can. J. Chem.* **1970**, *48*, 2866–2870.
(39) Sigel, H. Complex formation of nucleic bases with cupric ion. Acidity of N-1-protons in inosine-, guanosine-, uridine-, and thymidine 5′-triphosphates and their cupric complexes. *Eur. J. Biochem.* **1968**, *3*, 530–537.
(40) Sawyer, D. T.; Heineman, W. R.; Beebe, J. M. *Chemistry Experiments for Instrumental Methods*; John Wiley and Sons: New York, 1984; pp 19−23.
(41) Pozharskii, A. F. Heteroaromaticity. *Khim. Geterotsikl. Soedin.* **1985**, 867–905.
(42) Uhl, W.; Reiner, J.; Gassen, H. G. On the conformation of 5-substituted uridines as studied by proton magnetic resonance. *Nucleic Acids Res.* **1983**, *11*, 1167–1180.
(43) Burnstock, G.; Fischer, B.; Hoyle, C. H. V.; Maillard, M.; Ziganshin, A. U.; Brizzolara, A. L.; von Isakovics, A.; Boyer, J. L.; Harden, K.; Jacobson, K. A. Structure activity relationships for derivatives of adenosine-5′-triphosphate as agonists at P2 purinoceptors: heterogeneity within P2X and P2Y subtypes. *Drug Dev. Res.* **1994**, *31*, 206–219.
(44) Xie, D.; Li, A.; Wang, M.; Fan, Z.; Feng, H. LOCSVMPSI: a web server for subcellular localization of eukaryotic proteins using SVM and profile of PSI-BLAST. *Nucleic Acids Res.* **2005**, *33*, W105–W110.
(45) Ubl, J. J.; Vöhringer, C.; Reiser, G. Co-existence of two types of $[Ca^{2+}]_i$-inducing protease-activated receptors (PAR-1 and PAR-2) in rat astrocytes and C6 glioma cells. *Neuroscience* (*Oxford*) **1998**, *86*, 597–609.
(46) Ecke, D.; Tulapurkar, M. E.; Nahum, V.; Fischer, B.; Reiser, G. Opposite diastereoselective activation of $P2Y_1$ and $P2Y_{11}$ nucleotide receptors by adenosine 5′-O-(α-boranotriphosphate) analogues. *Br. J. Pharmacol.* **2006**, *149*, 416–423.
(47) Ecke, D.; Hanck, T.; Tulapurkar, M. E.; Schäefer, R.; Kassack, M.; Stricker, R.; Reiser, G. Hetero-oligomerization of the $P2Y_{11}$ receptor with the $P2Y_1$ receptor controls the internalization and ligand selectivity of the $P2Y_{11}$ receptor. *Biochem. J.* **2008**, *409*, 107–116.